Biochemistry and Biophysics Reports 33 (2023) 101433

Contents lists available at ScienceDirect

Biochemistry and Biophysics Reports

journal homepage: www.elsevier.com/locate/bbrep

Single-cell transcriptome analysis of a rat model of bilateral renal ischemia-reperfusion injury

Ayumu Taniguchi [a], Kazuya Miyashita [b], Shota Fukae [a], Ryo Tanaka [a], Mami Nishida [b,c], Tomomi Kitayama [b,c], Yuya Ouchi [b,c], Takashi Shimbo [c,d,**], Shigeaki Nakazawa [a], Kazuaki Yamanaka [a], Ryoichi Imamura [a], Katsuto Tamai [c,*], Norio Nonomura [a]

[a] Department of Urology, Osaka University Graduate School of Medicine, 2-2 Yamadaoka, Suita, Osaka, 565-0871, Japan
[b] StemRIM Inc., 7-7-15, Saito-Asagi, Ibaraki, Osaka, 567-0085, Japan
[c] Department of Stem Cell Therapy Science, Graduate School of Medicine, Osaka University, 2-2 Yamadaoka, Suita, Osaka, 565-0871, Japan
[d] StemRIM Institute of Regeneration-Inducing Medicine, Osaka University, 2-8 Yamadaoka, Suita, Osaka, 565-0871, Japan

ARTICLE INFO

Keywords:
Single cell
RNA sequencing
Acute kidney injury
Ischemia-reperfusion

ABSTRACT

Ischemia-reperfusion injury (IRI) causes massive tissue damage. Renal IRI is the most common type of acute renal injury, and the defects caused by it may progress to chronic kidney disease (CKD). Rodent models of renal IRI, with various patterns, have been used to study the treatment of human kidney injury. A rat model of bilateral IRI, in which the bilateral kidney blood vessels are clamped for 60 min, is widely used, inducing both acute and chronic kidney disease. However, the molecular mechanisms underlying the effects of bilateral IRI on kidney cells have not yet been fully elucidated. This study aimed to perform a whole-transcriptome analysis of the IRI kidney using single-cell RNA sequencing. We found renal parenchymal cells, including those from the proximal tubule, the loop of Henle, and distal tubules, to be damaged by IRI. In addition, we observed significant changes in macrophage population. Our study delineated the detailed cellular and molecular changes that occur in the rat model of bilateral IRI. Collectively, our data and analyses provided a foundation for understanding IRI-related kidney diseases in rat models.

1. Introduction

Blood supply is essential for maintaining tissue homeostasis. Immediate reperfusion is required when tissues encounter ischemic conditions. However, reperfusion after ischemia may sometimes evoke a detrimental outcome in tissues, which is known as ischemia-reperfusion injury (IRI) [1]. Although the detailed mechanisms underlying IRI are not fully understood yet, the involvement of oxidative stress from reactive oxygen species and various chemical mediators has been reported [2]. IRI has been described in multiple tissues, including the kidney, brain, lungs, heart, and liver. Acute kidney injury (AKI) caused by IRI leads to chronic kidney disease (CKD) [3,4]. IRI also occurs in the kidney at the time of renal transplantation, affecting its outcome [5,6]. Therefore, a detailed understanding of the mechanisms underlying IRI is essential, not only to elucidate its pathophysiology, but also to develop new therapeutic strategies.

Rodent models have been developed to analyze IRI in the kidneys [7,8]. One of the earliest models of IRI is the rat model in which bilateral kidney blood flow is cut off for 60 min followed by reperfusion [9]. In this model, intense tubular damages resulting in proteinuria as early as 16 weeks after reperfusion. In addition, transforming growth factor (TGF)-β1-dependent interstitial fibrosis develops approximately 40 weeks after reperfusion, and therefore, it can be used as a model for AKI-to-CKD transition [9]. Various renal IRI models with unilateral renal ischemia and/or with different ischemic times have been developed and used in various studies to elucidate the pathophysiology. However, a

* Corresponding author.
** Corresponding author. Department of Stem Cell Therapy Science, Graduate School of Medicine, Osaka University, 2-2 Yamadaoka, Suita, Osaka, 565-0871, Japan.
E-mail addresses: taniguchi@uro.med.osaka-u.ac.jp (A. Taniguchi), miyashita@stemrim.com (K. Miyashita), fukae@uro.med.osaka-u.ac.jp (S. Fukae), rtanaka@uro.med.osaka-u.ac.jp (R. Tanaka), nishida@stemrim.com (M. Nishida), kitayama@stemrim.com (T. Kitayama), ouchi@stemrim.com (Y. Ouchi), shimbot@sts.med.osaka-u.ac.jp (T. Shimbo), nakazawa@uro.med.osaka-u.ac.jp (S. Nakazawa), yamanaka@uro.med.osaka-u.ac.jp (K. Yamanaka), imamura@uro.med.osaka-u.ac.jp (R. Imamura), tamai@gts.med.osaka-u.ac.jp (K. Tamai), nono@uro.med.osaka-u.ac.jp (N. Nonomura).

https://doi.org/10.1016/j.bbrep.2023.101433
Received 21 October 2022; Received in revised form 19 January 2023; Accepted 20 January 2023

recent study suggested that the acute phase of IRI in the kidney could be impaired differently in humans and mice [7]. Thus, a comprehensive molecular-level understanding is essential to comprehend how the widely used rat model of renal bilateral 60-min ischemia-reperfusion injury could explain the changes in human pathology.

In this study, we aimed to perform single-cell RNA-sequencing (RNA-seq) in a rat model of renal bilateral ischemia to comprehensively analyze the gene expression profiles at a single-cell level. We attempted to identify the cells that are particularly impaired during ischemia-reperfusion and analyzed the cells contributing to the cellular impairment.

2. Materials and methods

2.1. Animals

All experiments were performed on six-week-old male Sprague-Dawley rats weighing 166–178 g, purchased from SLC Japan (Shizuoka, Japan) and maintained at the Institute of Experimental Animal Sciences of Osaka University Medical School. All animal studies were approved by the Osaka University Animal Research Committee (Permit No 03-032-003), according to the relevant regulatory standards.

2.2. Ischemia-reperfusion injury

The rats were randomly allocated to two groups, namely (i) sham operated (n = 4) and (ii) IRI (n = 5). Renal IRI or sham surgery was performed at six weeks of age, as described previously [10,11]. Briefly, rats were anesthetized with isoflurane and placed on heating pads to maintain their body temperature during surgery. A midline abdominal incision was made, and the bilateral renal pedicles were exposed and occluded with atraumatic microvascular clamps for 60 min. After the clamp was released, complete reperfusion was visually confirmed, and the incision was sutured (Fig. 1A). Sham surgery was performed identically, except for the renal pedicle clamping. Forty-eight hours after reperfusion, blood samples were collected from the tail vein, and serum creatinine levels were measured. To confirm that the degree of renal injury was consistent with established IRI data, two rats from each group were selected for renal specimen collection. The rats were euthanized, and blood, urine, and kidney samples were obtained. Before tissue collection, the kidneys were perfused by injecting saline through the left ventricle and debridement through an incision in the right atrium.

2.3. Histology

For histological evaluation, tissue samples extracted from rats were embedded in 4% paraformaldehyde. Four-micrometer-thick tissue sections were deparaffinized with xylene and stained with hematoxylin and eosin (HE). Histological slides were examined by light microscopy using a BZ-X710 microscope (Keyence, Osaka, Japan).

2.4. Serum creatinine quantification

Blood samples were collected from the tail vein immediately before kidney harvest, and serum creatinine levels were measured using a VetScan VS2 (Zoetis, Tokyo, Japan).

2.5. Library preparation for single-cell RNA-seq analysis

The left kidney of each rat (n = 2/group) was harvested and rinsed with Dulbecco's phosphate-buffered saline (DPBS; Nacalai, Kyoto, Japan). The renal capsule was removed and finely minced in a Petri dish

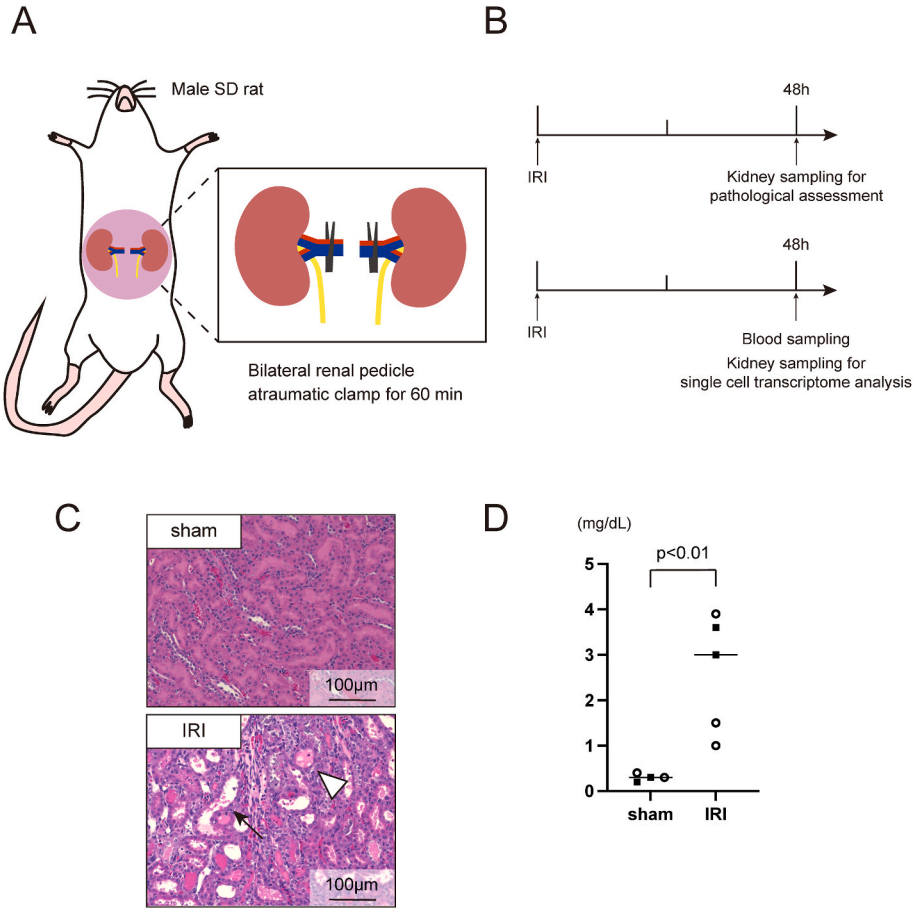

Fig. 1. Ischemia-reperfusion surgery (A) Schematic diagram illustrating the establishment of the rat model of bilateral ischemia-reperfusion. (B) Scheme showing time course of the experiment. Whole kidney specimens were used for single-cell transcriptome analysis, and pathological assessment was performed using identically treated rats. (C) Representative images of renal sections stained with hematoxylin and eosin 48 h after surgery in the sham and ischemia-reperfusion injury (IRI) groups. Acute pathological changes were observed in renal tissues of the IRI group. The black arrow indicates a dilated tubular with prolapse of tubular epithelial cells and loss of the brush border. The white arrowhead indicates cast formation. (D) Serum creatinine levels 48 h after surgery in the sham and IRI groups. Black square plots indicate the data of the rats subjected to single-cell transcriptome analysis.

on ice. Tissue pieces were placed in 5 mL of the solution from Multi Tissue Dissociation kit 2 (Miltenyi Biotec, Bergisch Gladbach, Germany) and digested using a gentleMACS Dissociator (Miltenyi Biotec). Dissociated cells were passed through a 70-μm cell strainer and centrifuged at 300×*g* for 5 min. The pellet was suspended in 30% Percoll (GE Healthcare, Chicago, IL, USA) and centrifuged at 700×*g* for 7 min. Cells were suspended in α-MEM (Thermo Fisher Scientific, Waltham, MA, USA) containing 2% fetal bovine serum and stained with CD45-APC/Cy7 antibody (BioLegend, San Diego, CA, USA). Dead cells were stained with SYTOX Blue Dead Cell Stain (Thermo Fisher Scientific) just before sorting. SYTOX-negative live cells and CD45-negative cells were sorted and collected using FACSAria III (BD Biosciences, Franklin Lakes, NJ, USA). Libraries were prepared using the Next GEM single cell 3′ kit (10 × Genomics, Pleasanton, CA, USA) according to the manufacturer's protocol (targeted 6000 cells for each sample).

2.6. Bioinformatics

Sequencing outputs were demultiplexed using 10 × Genomics Cell Ranger 6.0.0 [12] and bcl2fastq v2.20.0.422 (https://jp.support.illumina.com/sequencing/sequencing_software/bcl2fastq-conversion-software.html). The demultiplexed reads were aligned to the *Rattus norvegicus* reference genome (Rnor_6.0; Ensembl), and expression levels of transcripts were quantified using 10 × Genomics Cell Ranger. Count tables from Cell Ranger software were converted into Seurat objects using the "Read10X" and "CreateSeuratObject" command [13], after which cells harboring less than 200 UMIs and more than 50% mitochondrial genes were trimmed out from further analyses. Differentially expressed genes were obtained by the "FindMarkers" function built in the Seurat package, and gene ontology analysis was performed by the clusterProfiler package [14]. Data were visualized with dittoSeq [15] or Scanpy [16] using an h5ad file prepared by SeuratDisk (https://mojaveazure.github.io/eurat-disk/).

2.7. Statistical analysis

Serum creatinine levels between the two groups were compared using a nonpaired *t*-test and visualized with GraphPad Prism 9.5.0 (525).

3. Results

To dissect the cellular and molecular changes induced by IRI, we performed single-cell RNA-seq analysis of rat kidneys using the rat model of IRI (male, 6-week-old) as described above [10,11]. To confirm IRI, we analyzed the histology and plasma creatinine levels 48 h after reperfusion (Fig. 1B). Histological analysis identified massive damage such as tubular dilation, prolapse of tubular epithelial cells and cast formation. (Fig. 1C). Pathological changes of IRI in the left and right kidneys were comparable (Supplementary Fig. S1). Moreover, plasma creatinine levels in the IRI model group were significantly higher (2.60 mg/dL [95% confidence interval, 1.00–4.20 mg/dL]) than those in the sham group (0.30 mg/dL [0.17–0.43 mg/dL]; $p < 0.01$; Fig. 1D). Collectively, the data indicated the successful establishment of IRI in the rat model.

To comprehensively analyze the gene expression changes induced by IRI, we performed single-cell RNA-seq on the renal IRI model. Kidneys from the sham and rat models of IRI were enzymatically dissociated to isolate live and CD45$^-$cells (to focus on non-hematopoietic cells) using FACS (Supplementary Fig. S2). Single-cell RNA-seq libraries for live and CD45$^-$cells were prepared using Chromium Single Cell 3′ Gene Expression Solution (10 × Genomics) with the aim of recovering 6000 cells each. Downstream analyses were performed using combined data from live and CD45$^-$cells, unless specified otherwise. The basic quality scores after removing low-quality cells are shown in Fig. 2A. The samples from both sham and IRI models contained relatively high amounts of mitochondrial DNA transcripts, as previously described [17]. Thus, based on previous studies, we used a relaxed mitochondrial transcript filter (to remove the cells in which more than 50% of the transcripts were occupied by mitochondrial DNA-derived transcripts). After filtering, 11540 (live cells: 7269, CD45$^-$cells: 4271) and 8475 (live cells: 5826, CD45$^-$cells: 2649) cells were recovered from the sham and IRI models, respectively. Global gene expression profiles were visualized using a uniform manifold approximation and projection (UMAP) (Fig. 2B). The cell types in each cluster were annotated using known marker genes [18] (Fig. 2C). In addition to renal cells, we also identified macrophages (expressing *Adgre* and *Csf1r*), dendritic cells (expressing *Flt3*), neutrophils (expressing *S100a9* and *Mmp8*), T/NK cells (expressing *Cd3e* and *Klrb1c*), endothelial cells (expressing *Tek* and *Cdh5*), and myofibroblasts (expressing *Tagln* and *Acta2*). Cells from the sham and IRI models were differentially plotted on UMAP (Fig. 2D), which identified massive changes in gene expression profiles after IRI in hematopoietic cells and renal parenchymal cells including tubular cells and endothelial cells. The changes were particularly strong in tubular cells and macrophages.

To further understand the impact of IRI on renal cells, we specifically extracted the renal cells (CD45$^-$cells from Fig. 2B) and re-clustered them (Fig. 3A). Detailed cell-type annotation was performed using known marker genes (Fig. 3B) [18,19]. We successfully recovered the principal cells (expressing *Aqp2* and *Fxyd4*) and proximal tubule cells (expressing *Slc5a2* and *Slc13a1*), the loop of Henle (expressing *Slc12a1* and *Umod*), distal convoluted tubule cells (expressing *Slc12a3* and *Lhx1*), and collecting duct cells (expressing *Atp6v0d2* and *Atp6v1b1*). Cells from the sham and IRI models were labeled on UMAP (Fig. 3C). Interestingly, the proportion of most renal parenchymal cells significantly decreased after IRI, and only a portion of the proximal tubule cells remained. In addition, we observed SPP1-positive renal parenchymal cells, which were rarely detected in the sham data. Taken together, the data indicated that IRI caused massive and detrimental changes to the kidney.

Next, we evaluated changes in the macrophage population. We extracted the clusters expressing *Csf1r* or *Adgre1* (encoding the well-known macrophage marker F4/80), cells corresponding to clusters 1, 2, and 7 of the previous UMAP representation in Fig. 2B, and re-clustered them (Fig. 4A). Cells from the sham and IRI models were labeled on UMAP, showing a substantial difference in localization (Fig. 4B). We identified six different clusters, and the proportion of each cluster is shown in Fig. 4C. Since cluster 5 did not contain enough cells, it was omitted from further downstream analyses. Clusters 3 and 4 likely represented resident macrophages, since the complement genes, including *C1qa* and *C1qc*, were expressed (Fig. 4D). Cluster 4, expressing cell cycle-related genes, including *Mki67*, was predominantly occupied by cells from the IRI group, suggesting that the cells were undergoing rapid cell division in response to IRI-related inflammation (Fig. 4E). It was noteworthy that cluster 4 contained a fraction of cells expressing *Flt3*, but not the complement genes, suggesting that the cluster included fast-cycle dendritic cells, in addition to the resident macrophages (Supplementary Fig. S3). Cluster 0, strongly expressing *Cxcr4*, was dominant in the sham control but diminished in IRI (Fig. 4E). After IRI we observed two new clusters, cluster 1, weakly expressing *Cxcr4*, and cluster 2, expressing *Cd14* (Fig. 4E). Interestingly, cluster 1 expressed *Cd274* (also known as PD-L1), suggesting its involvement in IRI-induced anti-apoptotic effects [20,21] (Fig. 4E). Moreover, we found that cluster 2 expressed *Vcan*, which is involved in the establishment of fibrosis [22,23] (Fig. 4E). Together, the data indicated that macrophages dynamically repopulated upon IRI, and specific subtypes of macrophages that emerged upon IRI were inferred to be involved in IRI-induced cell death and fibrosis.

4. Discussion

Understanding the molecular mechanisms in renal IRI is critical, since IRI can induce CKD. In addition, renal transplantation inevitably results in IRI. Thus, in this study, we performed a whole-transcriptome

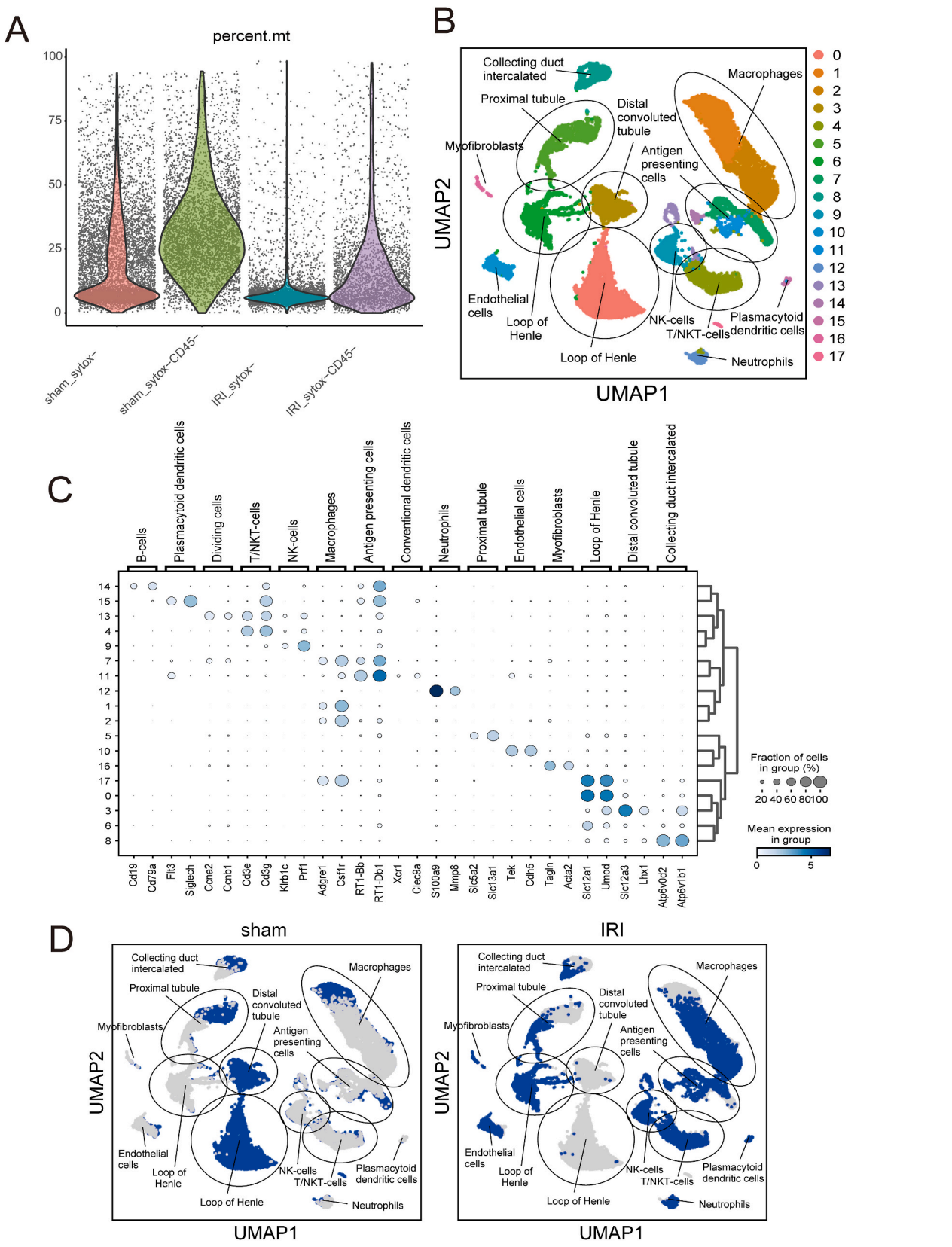

Fig. 2. Single-cell RNA-seq analysis using the ischemia-reperfusion injury (IRI) kidney (A) Violin plot showing the percentages of total mitochondrial transcripts. (B) Uniform Manifold Approximation and Projection showing the global gene expression signatures for each cell. Detected clusters were numbered and colored. (C) Dot plot showing the expression of marker genes. Color indicates the expression level of each gene. Size of dots indicates the fraction of cells expressing a particular gene in the cluster. (D) Cells from the sham or IRI model are differentially plotted. . (For interpretation of the references to color in this figure legend, the reader is referred to the Web version of this article.)

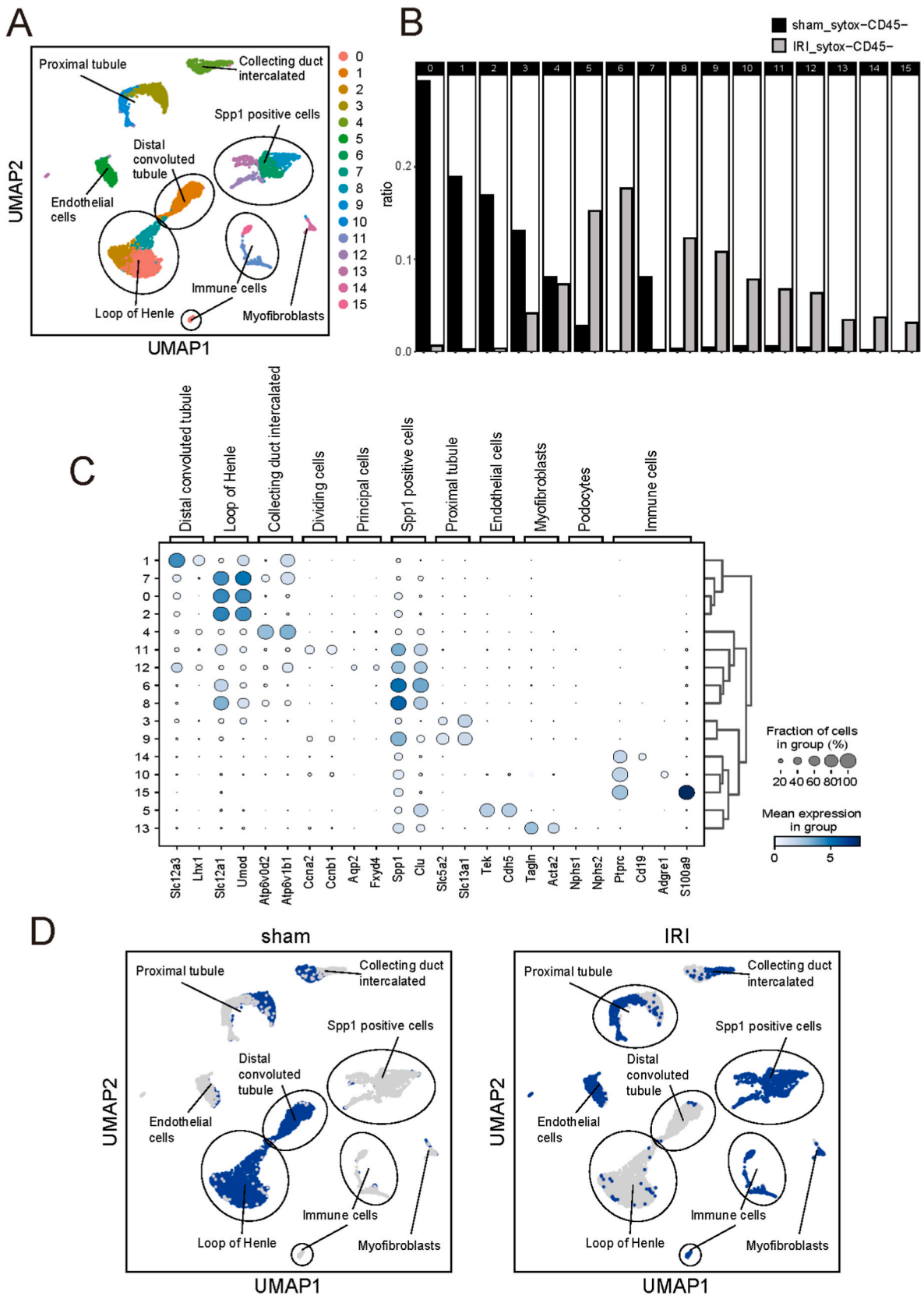

Fig. 3. Impact of ischemia-reperfusion injury (IRI) on the kidney parenchymal cells (A) UMAP shows the global gene expression signatures of kidney parenchymal cells. (B) Comparison of the proportions of each cluster between sham and IRI. (C) Dot plot shows the expression of marker genes. Color indicates the expression level of each gene. Size of dots indicates the fraction of cells expressing a particular gene in the cluster. (D) Cells from the sham or IRI model are differentially plotted. . (For interpretation of the references to color in this figure legend, the reader is referred to the Web version of this article.)

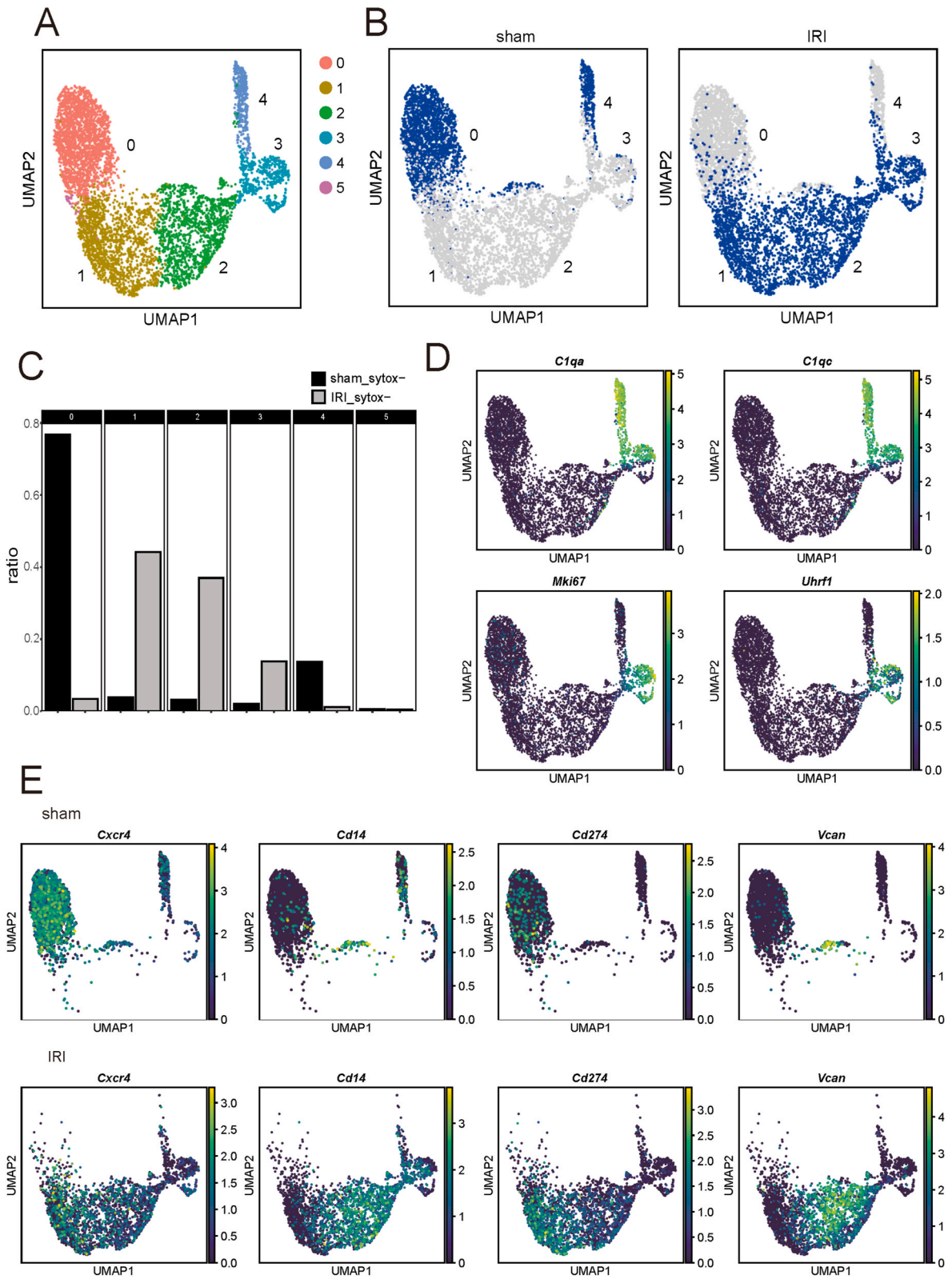

Fig. 4. Impact of ischemia-reperfusion injury (IRI) on the kidney macrophages (A) UMAP shows the global gene expression signatures of macrophages in the kidney. (B) Cells from the sham or IRI model were differentially plotted. (C) Comparison of the proportions of each cluster between sham and IRI. (D, E) Expression of each gene in the cells. The magnitude of expression is scaled and colored.

analysis of the kidney from a rat model of bilateral IRI using single-cell RNA-seq. Our data and analyses revealed that the renal tubules were severely damaged by bilateral IRI. Furthermore, infiltrating macrophages were found to drastically alter their gene expression status. Collectively, we identified that bilateral IRI in rats causes significant damage to the kidneys, the effects being mainly focused on renal tubules and macrophages.

Different types of IRI models, such as unilateral IRI, unilateral IRI

with contralateral nephrectomy, and bilateral IRI, are commonly used in animal experiments. In the unilateral IRI model, the contralateral kidney is intact and continuously functional. Therefore, compared to the bilateral IRI model, the unilateral IRI model allows long-term observation and is suitable for observing the transition from AKI to CKD [24]. However, the progression of renal failure over time is difficult to monitor using blood or urine samples, since the contralateral kidney functions in a compensatory manner. The unilateral IRI model with contralateral nephrectomy has better blood re-flow to the kidney after ischemia, thereby contributing to renal tissue recovery [25,26]. This model also has less renal fibrosis than a model without contralateral nephrectomy [27]. Typical causes of acute kidney injury in clinical practice include cardiac surgery and septic shock, which often result in bilateral kidney damage. In this respect, the bilateral IRI model resembles the pathophysiology of acute kidney injury in humans. Bilateral IRI models allow for long-term observation and exhibit events associated with the progression from AKI to CKD, such as fibrosis and proteinuria [27,28]. The factors that define renal injury from IRI are not limited to unilateral or bilateral inhibition. Varying the duration of renal ischemia can change the degree of damage, and some groups have reported different animal species, such as mice and humans, to have different outcomes induced by IRI [7,29]. Thus, an in-depth characterization of the model is critical to understand the extent to which it recapitulates human pathophysiology.

Analysis of renal parenchymal cells showed that IRI reduced the number of normal renal cells, and a population of cells expressing *Spp1* emerged. *Spp1* is a gene encoding the secreted phosphoprotein osteopontin, which is expressed in normal kidneys as well as bone [30]. Furthermore, it has been reported that osteopontin expression is increased in damaged kidneys [30,31]. One of the various functions of osteopontin is macrophage accumulation [32], and Shirakawa et al. reported that osteopontin is essential for both macrophage clearance of dead cells and promotion of fibrosis of the infarcted nest after myocardial infarction [33]. Therefore, Spp1 expression may be associated with the process by which injured cells are removed and tissue repair begins or fibrosis is established.

Detailed analysis of macrophage showed that the expression of *Cxcr4* was significantly altered by IRI. CXCR4 is the receptor for the leukocyte chemotactic factor SDF-1 [34]. Altered expression of *Cxcr4* in infiltrating macrophage clusters after IRI suggests altered chemotaxis of infiltrating macrophages. *Cd274*, also known as PD-L1, leads to T-cell apoptosis [20]. The increased expression of *Cd274* in infiltrating macrophages after IRI suggests the existence of a mechanism that acts in a suppressive manner on cellular immunity over-activated by IRI. Another macrophage cluster expressing *Cd14* and *Vcan* also appeared after IRI. CD14 on phagocytes recognizes lipopolysaccharides as a co-receptor for Toll-Like Receptor 4, which has also been reported to function in the removal of apoptotic cells by macrophage [35]. Interestingly, this CD14-mediated removal of apoptotic cells does not elicit inflammatory responses [35]. Versican is an extracellular matrix proteoglycan that is related to the establishment of renal fibrosis [22,23]. It is also an important molecule for leukocyte migration [36]. Since Versican can exhibit both pro- and anti-inflammatory effects through interactions with other cytokines [36], its significance in the post-IRI context is unclear, but it is likely to be related to the migration of leukocytes to the site of injury.

The results of the present study suggest an association between damaged renal parenchymal cells and macrophages in IRI. Renal parenchymal cells are assumed to signal to macrophages by increasing *Spp1* expression. As a result, macrophages undergo dynamic changes in cell proliferation, leukocyte migration, suppression of cellular immunity, and clearance of apoptotic cells.

One limitation of this study is that progression to CKD and renal fibrosis have not been evaluated. Various reports with different modeling methods have reported that renal fibrosis occurs a few weeks to several months after IRI [7]. How single-cell transcriptomes change in the chronic phase after IRI needs to be evaluated in future studies.

In this study, we provided comprehensive cellular and molecular profiles of bilateral IRI in rats. We specifically analyzed a model in which ischemia was limited to 60 min. Our data and analyses can support future studies to clarify the pathophysiology and develop effective therapies using the rat model of bilateral IRI.

Declaration of interest

The authors declare the following financial interests/personal relationships which may be considered as potential competing interests: Katsuto Tamai reports financial support was provided by StemRIM Inc. Katsuto Tamai reports a relationship with StemRIM Inc that includes: equity or stocks and funding grants. Katsuto Tamai reports a relationship with Shionogi and Co Ltd that includes: funding grants. Takashi Shimbo reports a relationship with StemRIM Inc that includes: equity or stocks. Kazuya Miyashita reports a relationship with StemRIM Inc that includes: employment and equity or stocks. Mami Nishida reports a relationship with StemRIM Inc that includes: employment and equity or stocks. Tomomi Kitayama reports a relationship with StemRIM Inc that includes: employment and equity or stocks. Yuya Ouchi reports a relationship with StemRIM Inc that includes: employment and equity or stocks. Corresponding author belongs to an endowment department funded by Shionogi and Co Ltd.-K.T.

Data availability

Data will be made available on request.

Acknowledgements

This work was supported by JSPS KAKENHI [grant number JP22K08690] and a research fund from StemRIM.

Appendix A. Supplementary data

Supplementary data to this article can be found online at https://doi.org/10.1016/j.bbrep.2023.101433.

References

[1] J.M. McCord, Oxygen-derived free radicals in postischemic tissue injury, N. Engl. J. Med. 312 (1985) 159–163, https://doi.org/10.1056/nejm198501173120305.
[2] E. Noiri, A. Nakao, K. Uchida, et al., Oxidative and nitrosative stress in acute renal ischemia, Am. J. Physiol. Ren. Physiol. 281 (2001) F948–F957, https://doi.org/10.1152/ajprenal.2001.281.5.F948.
[3] S.G. Coca, S. Singanamala, C.R. Parikh, Chronic kidney disease after acute kidney injury: a systematic review and meta-analysis, Kidney Int. 81 (2012) 442–448, https://doi.org/10.1038/ki.2011.379.
[4] M. Rahman, F. Shad, M.C. Smith, Acute kidney injury: a guide to diagnosis and management, Am. Fam. Physician 86 (2012) 631–639.
[5] N. Perico, D. Cattaneo, M.H. Sayegh, G. Remuzzi, Delayed graft function in kidney transplantation, Lancet 364 (2004) 1814–1827, https://doi.org/10.1016/s0140-6736(04)17406-0.
[6] C. Ponticelli, Ischaemia-reperfusion injury: a major protagonist in kidney transplantation, Nephrol. Dial. Transplant. 29 (2014) 1134–1140, https://doi.org/10.1093/ndt/gft488.
[7] Y. Fu, C. Tang, J. Cai, et al., Rodent models of AKI-CKD transition, Am. J. Physiol. Ren. Physiol. 315 (2018) F1098–F1106, https://doi.org/10.1152/ajprenal.00199.2018.
[8] N. Shiva, N. Sharma, Y.A. Kulkarni, et al., Renal ischemia/reperfusion injury: an insight on in vitro and in vivo models, Life Sci. 256 (2020), 117860, https://doi.org/10.1016/j.lfs.2020.117860.
[9] D.P. Basile, D. Donohoe, K. Roethe, J.L. Osborn, Renal ischemic injury results in permanent damage to peritubular capillaries and influences long-term function, Am. J. Physiol. Ren. Physiol. 281 (2001) F887–F899, https://doi.org/10.1152/ajprenal.00050.2001.
[10] H. Nasrallah, I. Aissa, C. Slim, et al., Effect of oleuropein on oxidative stress, inflammation and apoptosis induced by ischemia-reperfusion injury in rat kidney, Life Sci. 255 (2020), 117833, https://doi.org/10.1016/j.lfs.2020.117833.
[11] E. Oztas, A. Guven, E. Turk, et al., 3-aminobenzamide, a poly ADP ribose polymerase inhibitor, attenuates renal ischemia/reperfusion injury, Ren. Fail. 31 (2009) 393–399, https://doi.org/10.1080/08860220902882741.

[12] G.X. Zheng, J.M. Terry, P. Belgrader, et al., Massively parallel digital transcriptional profiling of single cells, Nat. Commun. 8 (2017), 14049, https://doi.org/10.1038/ncomms14049.
[13] D. Sacks, B. Baxter, B.C.V. Campbell, et al., Multisociety consensus quality improvement revised consensus statement for endovascular therapy of acute ischemic stroke, Int. J. Stroke 13 (2018) 612–632, https://doi.org/10.1177/1747493018778713.
[14] T. Wu, E. Hu, S. Xu, et al., clusterProfiler 4.0: a universal enrichment tool for interpreting omics data, Innovation 2 (2021), https://doi.org/10.1016/j.xinn.2021.100141.
[15] D.G. Bunis, J. Andrews, G.K. Fragiadakis, et al., dittoSeq: universal user-friendly single-cell and bulk RNA sequencing visualization toolkit, Bioinformatics 36 (2020) 5535–5536, https://doi.org/10.1093/bioinformatics/btaa1011.
[16] F.A. Wolf, P. Angerer, F.J. Theis, SCANPY: large-scale single-cell gene expression data analysis, Genome Biol. 19 (2018) 15, https://doi.org/10.1186/s13059-017-1382-0.
[17] B.R. Conway, E.D. O'Sullivan, C. Cairns, et al., Kidney single-cell atlas reveals Myeloid heterogeneity in progression and regression of kidney disease, J. Am. Soc. Nephrol. 31 (2020) 2833–2854, https://doi.org/10.1681/asn.2020060806.
[18] Z. Miao, M.S. Balzer, Z. Ma, et al., Single cell regulatory landscape of the mouse kidney highlights cellular differentiation programs and disease targets, Nat. Commun. 12 (2021) 2277, https://doi.org/10.1038/s41467-021-22266-1.
[19] V. Saxena, H. Gao, S. Arregui, et al., Kidney intercalated cells are phagocytic and acidify internalized uropathogenic Escherichia coli, Nat. Commun. 12 (2021) 2405, https://doi.org/10.1038/s41467-021-22672-5.
[20] P.C. Tumeh, C.L. Harview, J.H. Yearley, et al., PD-1 blockade induces responses by inhibiting adaptive immune resistance, Nature 515 (2014) 568–571, https://doi.org/10.1038/nature13954.
[21] Y. Iwai, S. Terawaki, M. Ikegawa, et al., PD-1 inhibits antiviral immunity at the effector phase in the liver, J. Exp. Med. 198 (2003) 39–50, https://doi.org/10.1084/jem.20022235.
[22] M. Rudnicki, P. Perco, H. Neuwirt, et al., Increased renal versican expression is associated with progression of chronic kidney disease, PLoS One 7 (2012), e44891, https://doi.org/10.1371/journal.pone.0044891.
[23] R. Han, S. Hu, W. Qin, et al., C3a and suPAR drive versican V1 expression in tubular cells of focal segmental glomerulosclerosis, JCI Insight 4 (2019), https://doi.org/10.1172/jci.insight.122912.
[24] N. Le Clef, A. Verhulst, P.C. D'Haese, B.A. Vervaet, Unilateral renal ischemia-reperfusion as a robust model for acute to chronic kidney injury in mice, PLoS One 11 (2016), e0152153, https://doi.org/10.1371/journal.pone.0152153.
[25] W.F. Finn, Enhanced recovery from postischemic acute renal failure. Micropuncture studies in the rat, Circ. Res. 46 (1980) 440–448, https://doi.org/10.1161/01.res.46.3.440.
[26] W.F. Finn, E. Fernandez-Repollet, D. Goldfarb, et al., Attenuation of injury due to unilateral renal ischemia: delayed effects of contralateral nephrectomy, J. Lab. Clin. Med. 103 (1984) 193–203.
[27] L. Yang, T.Y. Besschetnova, C.R. Brooks, et al., Epithelial cell cycle arrest in G2/M mediates kidney fibrosis after injury, Nat. Med. 16 (535–543) (2010), https://doi.org/10.1038/nm.2144, 531p following 143.
[28] D.P. Basile, D. Donohoe, K. Roethe, J.L. Osborn, Renal ischemic injury results in permanent damage to peritubular capillaries and influences long-term function, Am. J. Physiol. Ren. Physiol. 281 (2001) F887–F899, https://doi.org/10.1152/ajprenal.2001.281.5.F887.
[29] Y. Dong, Q. Zhang, J. Wen, et al., Ischemic duration and frequency determines AKI-to-CKD progression monitored by dynamic changes of tubular biomarkers in IRI mice, Front. Physiol. 10 (2019) 153, https://doi.org/10.3389/fphys.2019.00153.
[30] D.T. Denhardt, X. Guo, Osteopontin: a protein with diverse functions, Faseb. J. 7 (1993) 1475–1482.
[31] V. Rudman-Melnick, M. Adam, A. Potter, et al., Single-cell profiling of AKI in a murine model reveals novel transcriptional signatures, profibrotic phenotype, and epithelial-to-stromal crosstalk, J. Am. Soc. Nephrol. 31 (2020) 2793–2814, https://doi.org/10.1681/ASN.2020010052.
[32] S.R. Rittling, D.T. Denhardt, Osteopontin function in pathology: lessons from osteopontin-deficient mice, Exp. Nephrol. 7 (1999) 103–113, https://doi.org/10.1159/000020591.
[33] K. Shirakawa, J. Endo, M. Kataoka, et al., IL (Interleukin)-10-STAT3-Galectin-3 Axis is essential for osteopontin-producing reparative macrophage polarization after myocardial infarction, Circulation 138 (2018) 2021–2035, https://doi.org/10.1161/circulationaha.118.035047.
[34] M.E. Bianchi, R. Mezzapelle, The chemokine receptor CXCR4 in cell proliferation and tissue regeneration, Front. Immunol. 11 (2020), https://doi.org/10.3389/fimmu.2020.02109.
[35] C.D. Gregory, CD14-dependent clearance of apoptotic cells: relevance to the immune system, Curr. Opin. Immunol. 12 (2000) 27–34, https://doi.org/10.1016/s0952-7915(99)00047-3.
[36] T.N. Wight, I. Kang, S.P. Evanko, et al., Versican—a critical extracellular matrix regulator of immunity and inflammation, Front. Immunol. 11 (2020), https://doi.org/10.3389/fimmu.2020.00512.